The 10th International Symposium on Flow Visualization
August 26-29, 2002, Kyoto, Japan
F0002

Particle-Flow CT Images Decomposed with 3D Wavelets

Visualization of Front and Rear of Dense Flow at Bend Upstream

Takei,M.*[1] Li,H.*[2] Ochi,M.*[1] Saito,Y.*[3] and Horii,K.*[4]

*1 Department of Mechanical Engineering, Nihon University,
1-8-14 KandaSurugadai, Chiyoda, Tokyo, 101-8308, Japan
Tel:+81-3-3259-0749 / FAX:+81-3-3293-8254
E-mail: takei@mech.cst.nihon-u.ac.jp
*2 Kagoshima University, Kagoshima Japan
*3 Hosei University, Tokyo Japan
*4 Shirayuri College, Tokyo Japan

Abstract: Particle flow CT images at the upstream of a bend pipe is decomposed to the time levels to extract dominant particle density distribution using three-dimensional discrete wavelets transform. As a result, the high density of the particle spatial distribution at the front of a dense flow, which composes high time frequency level, is located at the upper part than that just over the stationary layer. It reveals that the particles composing the plug at the front are steep and are discharged toward the front air phase. Moreover, the particle density at the rear of the dense flow moves from the level 5 to the level 7; then, the dominant spatial part moves from the top to the bottom as the time passes. It indicates the dense flow formation, whose rear is gently slope.

Keywords: CT, Solid-air two phase flow, Particle conveyance, Wavelets transform

1. Introduction

Dense flow in a pipeline has been typically used in various industries such as a chemical, a pharmaceutical, and a food industries. The basic physical properties of the dense flow should be measured in order to provide the predictive mechanism for the pipeline design. The particle movement of the dense plug flow is visualized by a high-speed camera (Klinzing G.E, 2001); it reveals qualitatively the particle flow within the plug from the pickup at the beginning to the falling off at the end. Moreover, quantitatively, velocities of particles composing a plug front end was measured at cross-sectional grids in a pipeline by means of LDV to discuss the movement patterns of the particles (Takei,M et al. 1998). However, the LDV method cannot measure the entire cross section; therefore, it is difficult to understand the three-dimensional (two spatial dimension and one time dimension) particle movement in a dense flow.

Under these circumstances, capacitance CT together with real time visualization has been studied as a technique by which to visualize particle behavior in a cross section of a pipeline (Huang,S.M. et al. 1989; Dyakowski,T. et al. 1999). This capacitance CT arranges a sensor consisting of many electrodes around the circumference of a pipeline in order to measure the capacitances between the electrodes. The distribution of particle density based on the permittivity distribution on the cross section is obtained via a reconstruction method. However, the images obtained by the capacitance CT are blurred because the approximate values are resolved using a mathematical ill-posed inverse problem. Image analysis is necessary in order to extract the features of the blurred images in order to ascertain the dominant particles from the image.

Currently, in mechanical engineering fields, wavelets transform is being performed using image analysis rather than Fourier transform. The merits of wavelets analysis is the ability to analyze the frequency, while not removing time information. The discrete wavelets transform has been used primarily for picture image processing. The orthonormal transform of this analysis enables quantitative decomposition and recomposition of a picture image. A number of researchers applied this idea to the analysis of a jet image (Li,H, et al.,1999). Generally, two-dimensional wavelets transform has been used to obtain the two dimensional original image.

The originality of the present method lies in the application of three-dimensional discrete wavelets transform to a three-dimensional capacitance CT image in order to extract the particle pattern features in a particle dense flow at the upstream of a bend pipe. In the present study, particle capacitances upstream of a pipe bend are measured to re-construct the particle density images using two-dimensional space and time. The images are transformed by three-dimensional discrete wavelets in order to extract the dominant time particle levels.

2. 3D Discrete Wavelets Transform

The three-dimensional wavelets spectrum $\mathbf{S}_{tyx}$ is obtained by

$$\mathbf{S}_{tyx} = [\mathbf{W}_t[\mathbf{W}_y[\mathbf{W}_x\mathbf{E}_{xyt}]^T]^T]^T \tag{1}$$

where, $\mathbf{E}_{xyt}$ is a three-dimensional original image consisting of Nx×Ny×Nt pixels. Nx, Ny and Nt are pixels in the x, y (space axis) and t (time axis) dimensions, respectively, $\mathbf{W}_x$, $\mathbf{W}_y$ and $\mathbf{W}_t$ are the analyzing wavelet matrices consisting of Nx×Nx pixels, Ny×Ny pixels and Nt×Nt pixels, respectively. The transpose matrices are defined as

$$[\mathbf{E}_{xyt}]^T = \mathbf{E}_{txy} \qquad [\mathbf{E}_{txy}]^T = \mathbf{E}_{ytx} \qquad [\mathbf{E}_{ytx}]^T = \mathbf{E}_{xyt} \tag{2}$$

Therefore, the wavelets spectrum $\mathbf{S}_{tyx}$ is composed of Nt×Ny×Nx pixels. The inverse three dimensional wavelets transform of Eq. (1) is expressed as

$$\mathbf{E}_{xyt}=[\mathbf{W}_x[\mathbf{W}_y[\mathbf{W}_t\,\mathbf{S}_{tyx}]^T]^T]^T \tag{3}$$

For 2nd-order Daubechies orthonormal functions of the analyzing wavelets, and original image data consisting of Nx=Ny=32, Nt=512, an original image can be decomposed to each frequency the level as shown in Fig.1, namely,

$$\mathbf{E}_{xyt}= \mathbf{E}_0 + \mathbf{E}_1 + \mathbf{E}_2 + \mathbf{E}_3 + \mathbf{E}_4 + \mathbf{E}_5 + \mathbf{E}_6 + \mathbf{E}_7 + \mathbf{E}_8 + \mathbf{E}_9$$

$$\mathbf{E}_0=[\mathbf{W}_x[\mathbf{W}_y[\mathbf{W}_t\mathbf{S}_0]^T]^T]^T \qquad \mathbf{E}_1=[\mathbf{W}_x[\mathbf{W}_y[\mathbf{W}_t\mathbf{S}_1]^T]^T]^T \qquad \mathbf{E}_2=[\mathbf{W}_x[\mathbf{W}_y[\mathbf{W}_t\mathbf{S}_2]^T]^T]^T$$

$$\mathbf{E}_3=[\mathbf{W}_x[\mathbf{W}_y[\mathbf{W}_t\mathbf{S}_3]^T]^T]^T \qquad \mathbf{E}_4=[\mathbf{W}_x[\mathbf{W}_y[\mathbf{W}_t\mathbf{S}_4]^T]^T]^T \qquad \mathbf{E}_5=[\mathbf{W}_x[\mathbf{W}_y[\mathbf{W}_t\mathbf{S}_5]^T]^T]^T$$

$$\mathbf{E}_6=[\mathbf{W}_x[\mathbf{W}_y[\mathbf{W}_t\mathbf{S}_6]^T]^T]^T \qquad \mathbf{E}_7=[\mathbf{W}_x[\mathbf{W}_y[\mathbf{W}_t\mathbf{S}_7]^T]^T]^T \qquad \mathbf{E}_8=[\mathbf{W}_x[\mathbf{W}_y[\mathbf{W}_t\mathbf{S}_8]^T]^T]^T$$

$$\mathbf{E}_9=[\mathbf{W}_x[\mathbf{W}_y[\mathbf{W}_t\mathbf{S}_9]^T]^T]^T \tag{4}$$

where, $\mathbf{S}_0$ is the lowest frequency spectrum, and $\mathbf{S}_5$ is the highest frequency spectrum. Therefore, $\mathbf{E}_0$, the image inversely transformed from $\mathbf{S}_0$, indicates the particle two-dimensional space distribution having the lowest time frequency, which is referred to as time level 0. Thus, time level 0 indicates the time mean space distribution. On the other hand, $\mathbf{E}_9$, the image inversely transformed from $\mathbf{S}_9$, indicates the two-dimensional space distribution having the highest time frequency, which is referred to as time level 9. Time level 9 therefore indicates the most time-fluctuated space distribution. Fig.2 shows the matrix element values of the analyzing wavelet matrix of Daubechies function of 2nd order in the case of 32 pixels, which is $\mathbf{W}_x$ and $\mathbf{W}_y$. The matrix element values in the case of 512 pixels, which is $\mathbf{W}_t$, are obtained by magnification of the Fig.2. Fig.3 shows the power spectrum of the analyzing wavelet of Daubechies function of 2nd order. The relationship between wavelet levels and the representative space frequencies obtained from the absolute values by Fourier transform is shown in Table 1 for the case of Δt = 10 ms. The representative time frequency is the frequency indicating the highest value in the band of the wavelet level. The each level operates a kind of band pass filter.

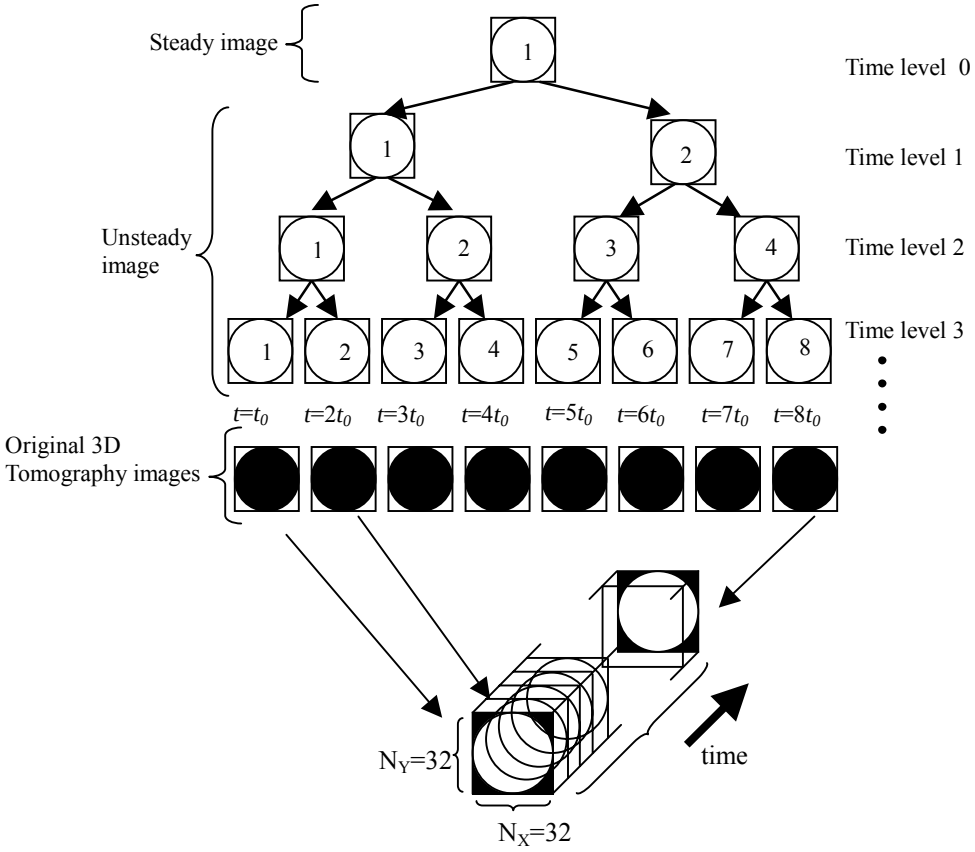

Fig.1 Multiresolution by 3D wavelets

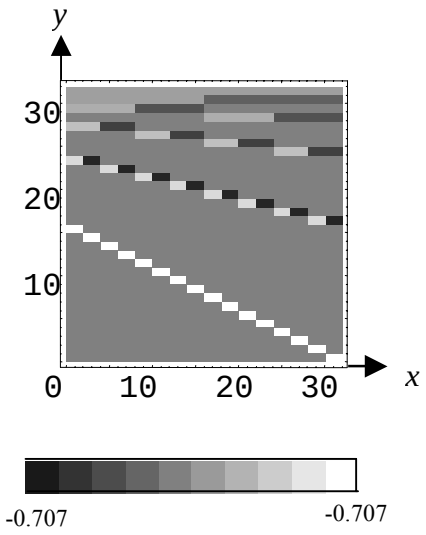

Fig.2 Analyzing wavelet matrix

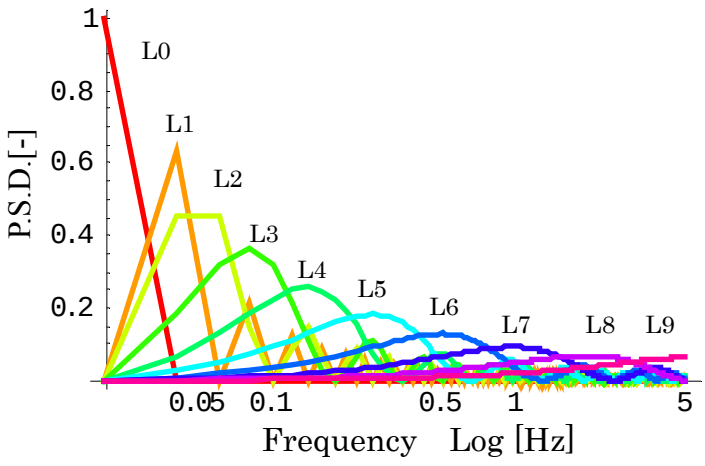

Fig.3 Power spectrum of analyzing wavelet

Table 1 Relationship between wavelet levels and representative frequency

Time level	Time Frequency [Hz]	Mean Frequency [Hz]
0	0.150～0.195	0.17
1	0.195～0.390	0.29
2	0.390～0.586	0.49
3	0.586～0.781	0.68
4	0.781～1.953	1.37
5	1.953～3.320	2.64
6	3.320～7.227	5.27
7	7.227～14.84	11.03
8	14.84～30.85	22.85
9	30.85～50.00	40.3

3. Principle of Capacitance Tomography

The capacitance CT sensor is set up at the circumference of a pipeline, as shown in Figs. 4(A) and (B). Insulation materials separate the 12 electrodes in the sensor. The relationship between capacitance and permittivity in the static electro field is expressed by

$$C_{i,j} = -\frac{\varepsilon_0}{V_c} \oint_{r \subseteq \Gamma_j} \varepsilon(\mathbf{r}) \nabla V_i(\mathbf{r}) \bullet d\mathbf{r} \qquad (5)$$

where i is a standard electrode number from 1 to 11, and j is a reference electrode number from i+1 to 12. $C_{i,j}$ is the capacitance between the standard electrode i and the reference electrode j, ε_0 is the vacuum permittivity of air, and $\varepsilon(\mathbf{r})$ is the permittivity distribution on the cross section. $\mathbf{r}$ is a position vector on the cross section. V_c is the voltage across the i^{th} electrode. Γ_j is the area affected by the electric line of force. $V_i(\mathbf{r})$ is the potential distribution on the cross section between the i^{th} and j^{th} electrodes. Since $V_i(\mathbf{r})$ is unknown in Eq.(5), the Laplace equation

$$\nabla \bullet [\varepsilon(\mathbf{r}) \nabla V(\mathbf{r})] = 0 \qquad (6)$$

is assumed on the cross section. $V(\mathbf{r})$ is obtained from the discretized Eq.(6). The matrix expression in Eq.(5) showing the relation between the capacitance matrix **C** and the permittivity distributions **E** is

$$\mathbf{C} = \mathbf{S_e E} \qquad (7)$$

where the sensitivity map matrix S_e consists of the known values of ε_0, V_c and $\nabla V_i(\mathbf{r})$ in Eq.(5). In other words, the capacitance CT provides a means by which to obtain the permittivity distribution of particles **E** on the cross section from both the known sensitivity map matrix $\mathbf{S_e}$ and the measured capacitance matrix **C**. In the case of the 12 electrodes, the sensitivity map $\mathbf{S_e}$ is a 66×1024 matrix in Eq.(7). Here, the capacitance matrix **C** expresses a 66×1 matrix, and the permittivity distribution matrix **E** is a 1024×1 matrix for the case in which the pipeline cross-section is divided by a 32×32 = 1024 square mesh. The mathematical method used to obtain the permittivity matrix **E** from the capacitance matrix **C** and the sensitivity map matrix $\mathbf{S_e}$ are an ill posed inverse problem because the inverse matrix $\mathbf{S_e}^{-1}$ does not exist. The image is re-constructed by the back projection method.

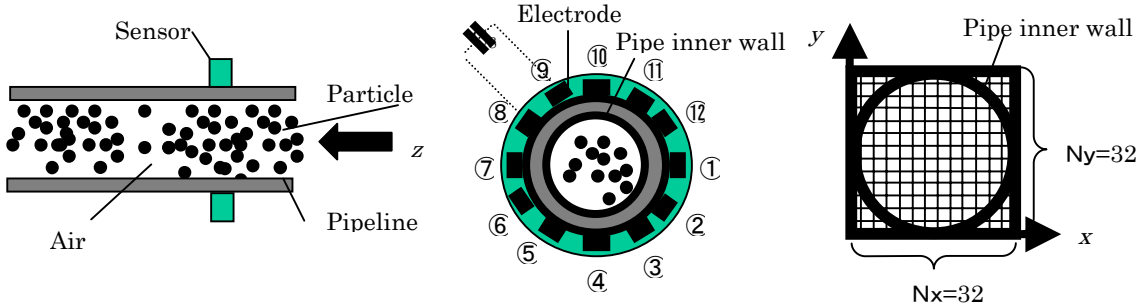

(a) Front view (b) Cross view (c) Space resolution

Fig. 4 Overview of capacitance tomography and associated space resolution

4. Experiments

4.1 Experimental Equipment, Conditions & Method

The equipment for the present experiment consisted of a feeder tank, a pipeline of 49.0 mm inside diameter, a receiver tank and a Root's blower, as shown in Fig. 5. A CT sensor having 12 electrodes was arranged around the pipe circumference upstream of the pipe bend. The air suction volume was 0.019 m^3/s, and the particle was supplied at 390.0 g/s. The mean air velocity in the pipeline as calculated from the air volume was 9.10 m/s. The Reynolds number was 2.92×10^4. The solid air ratio was 12.46. The particles were polyethylene pellets, which were almost spherical, having a 3.26-mm diameter and a density of 910 kg/m^3. The time interval necessary to acquire one frame is Δt = 10.0 ms. The 512 consecutive frames for 5,120.0 ms are selected from among the total reconstructed frames obtained for 60.0 seconds for analysis in the next section.

In the present study, the permittivity matrix, **E**, which indicates the particle two-dimensional space distribution at a time, is normalized via a calibration using the maximum value of 1.0 and the minimum value of 0.0. The maximum value indicates the situation whereby the particles occupy the entire cross-section. The minimum value indicates the situation whereby the air occupies the entire cross-section. One image pixel is 1.53×1.53 mm^2. The inside cross-section 49.0 mm is divided by 32×32 image pixels. When a particle core passes through the measurement section, the diameter of one particle takes up 2.13 image pixels because the particle diameter is 3.26 mm. Accurately, this sensor obtains the particle density distribution in a cell Δz × one-image pixel for Δt. The flow direction length of the sensor Δz = 63.0 mm. The particle distance for Δt is approximately $v_p \Delta t$ = 91.0mm (the particle mean velocity v_p is assumed to be the mean air velocity).

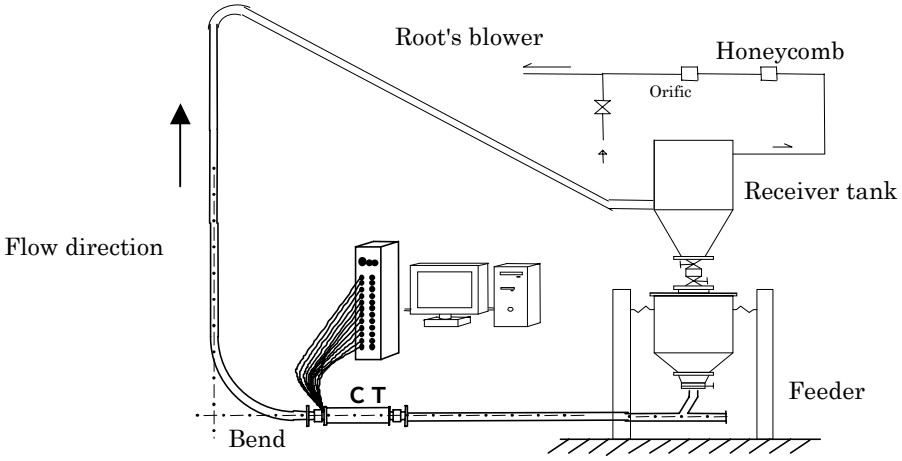

Fig.5 Experimental equipment

4.2 Experimental Results

The reconstructed three-dimensional image obtained by the CT, $\mathbf{E}_{xyt,}$ is re-calculated to obtain the density image, $\mathbf{E'}_{xyt}$ by dividing by the root mean square value,

$$\mathbf{E'}_{xyt} = \frac{(\mathbf{E}_{xyt} - \bar{\mathbf{E}})}{\mathbf{E}_{RMS}} \tag{8}$$

where, $\mathbf{E'}_{xyt}$ is the distribution of the particle density at a point located at x, y, and t in a cell, Δz × one image pixel for Δt. The root mean square and the time mean values are calculated by

$$\mathbf{E}_{RMS} = \frac{1}{N_t N_y N_x} \sum_{t=1}^{Nt} \sum_{y=1}^{Ny} \sum_{x=1}^{Nx} \sqrt{\left(\mathbf{E}_{xyt} - \bar{\mathbf{E}}\right)^2} \qquad \bar{\mathbf{E}} = \frac{1}{N_t N_y N_x} \sum_{t=1}^{Nt} \sum_{y=1}^{Ny} \sum_{x=1}^{Nx} \mathbf{E}_{xyt} \tag{9}$$

The representative particle density images $\mathbf{E'}_{xyt}$ from $50\Delta t$ to $500\Delta t$ at $50\Delta t$ step (Δt = 10 ms) are

shown in Fig. 6. The image pixel, at which no particle exists, is blue. As the particle density on an image pixel becomes high, the image pixel turns red as shown in the color bar. At the upstream of a bend pipe, particles in the dense flow are accumulated resulting in the plug flow. Form Fig.6, on the whole, the time transient distributions of the particle density are qualitatively visualized. In order to confirm roughly the particle movement during the time, the spatial mean particle density at a time are calculated by

$$\overline{D_p}(t) = \frac{1}{N_y N_x} \sum_{y=1}^{Ny} \sum_{x=1}^{Nx} \mathbf{E}_{xy}(t) \tag{10}$$

to show in Fig.7. This figure reveals that five dense flows passed through the pipe cross section during the time (denote 1,2 3,4 and 5), and three dense flows 1,2 and 3 plug the pipe cross section entirely; however, two dense flows 4 and 5 do not plug the pipe cross section because the value is low. In the next section, the highly dense flow 1, 2 and 3 are analyzed by three dimensional wavelet multiresolution.

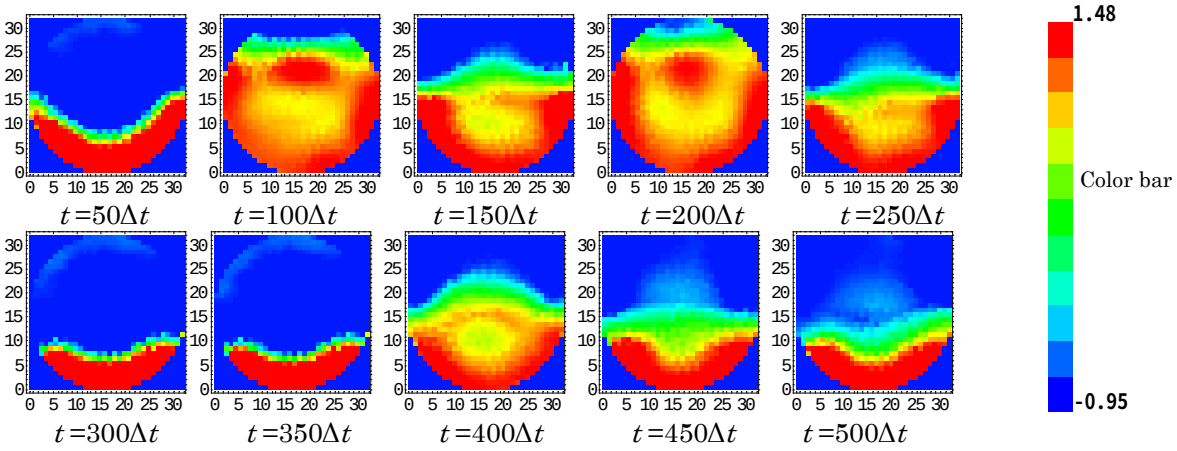

Fig.6 Representative Images

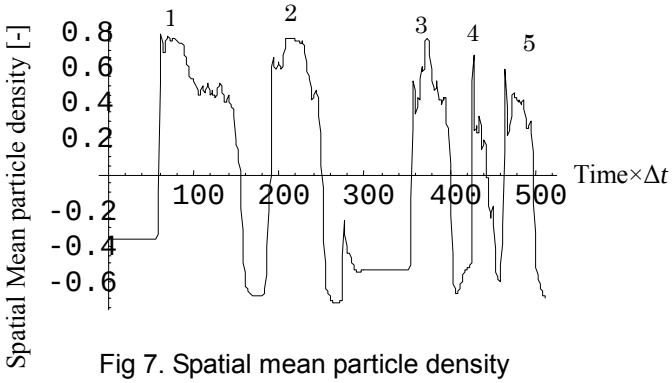

Fig 7. Spatial mean particle density

5. Analysis and Discussion

5.1 Wavelets Multiresolution to Time

The three-dimensional original images of the particle density in Fig.6 are decomposed by three dimensional wavelet multiresolution of Eqs.(1), (3) and (4). The values outside the pipe wall are replaced with the lowest value to clarify the images. The lowest time frequency of the time level 0 indicates the steady two-dimensional space distribution of the particle density during the time. The highest time frequency of the time level 9 indicates the least steady distribution of the particle density. Fig.8 shows the example of the decomposed images from the original image at 100Δ*t*, which is the middle part of the dense flow 1 according to Fig.7. The color map values are different

among the original, the level 0 and the more than the level 1 images. The summation of all level images at each space element completely recovers the original image in Fig.8 due to the orthonormal wavelets transform. From Fig.8, the lowest frequency level 0 indicates the time-mean particle density spatial distribution; namely, the distribution is mainly a stationary layer, which is located at the pipeline bottom. Also, the figure 8 reveals that the relative low frequency level 3 dominates the particle movement at $100\Delta t$ among these levels, and the spatial particle distribution in the level 3 is located above the stationary layer of the time-mean location in the level 0. Moreover, in the levels 1 and 2, both sides above the stationary layer have slight yellow parts (denote A), indicating the particle density is changed at these parts with low frequency. And then, yellow parts are slightly visible at the upper part of the cross section in the levels 6 and 7 (denote B). It means particles densities at the upper part are changed slightly with high frequency.

In order to confirm dominant levels of the total particle movement, the spatial-mean values of the particle density images decomposed by the wavelets multiresolution are calculated by

$$\overline{D_p^L}(t,L) = \frac{1}{N_y\, N_x} \sum_{y=1}^{Ny} \sum_{x=1}^{Nx} \mathbf{E}_{xy}^{L}(t,L) \tag{11}$$

$\mathbf{E}_{xy}^{L}(t,L)$ is the level L image decomposed by the multiresolution at the time t.

Figure 9 is the results from the level 0 to the level 7. The levels 8 and 9 are omitted because the levels do not clearly appear a peak. In the level 3, three high values to denote 1, 2 and 3 are visible at the period from $65\Delta t$ to $128\Delta t$, from $193\Delta t$ to $250\Delta t$, and from $354\Delta t$ to $384\Delta t$, which are equivalent to the numbers in Fig.7. The particle density of each level at the start and end times of those periods are visualized to discuss the particle movement in detail. First, the period 1 is discussed. Just before the start time; at $64\Delta t$, in the levels 6 and 7, a high value is appeared (denote 1-s), which indicates the front of the start time. At the end time of the period 1; $132\Delta t$, in the levels 4 and 5, a high value is appeared (denote1-e). As the time goes, at $148\Delta t$ in the levels 6 and 7, a high value is appears, and the high value moves to $156\Delta t$ in the level 7 (denote 1-e). Next, the period 2 is discussed. At $192\Delta t$ in the levels 6 and 7, a high value is appeared (denote 2-s). At the end time of the period 2; $240\Delta t$, the high value is slightly appeared (denote 2-e) in the level 5. As the time goes, at $243\Delta t$ in the level 6 (denote 2-e), a high value is appeared, and the high value moves to $250\Delta t$ in the level 7 (denote 2-e). Finally, the period 3 is discussed. From $354\Delta t$ in the level 4, a high value is appeared (denote 3-s), the period is included in the period 3 in the level 3. Therefore, at the period 3, the level 4 is dominant rather than the level 3 in terms of the low frequency. At the start time near $354\Delta t$, the high level such as the levels 6 and 7 do not a high value. At the end time; $384\Delta t$ in the level 5 (denote 3-e), a high value is appeared. As the time goes, the high value moves to $400\Delta t$ in the level 6, $402\Delta t$ in the level 7 (denote 3-e). The above discussion reveals that at the start time of each period, a high value is appeared in the higher level; the high value moves to higher level as the time passes.

Next, the start and end times of the three period are focused to confirm the flow pattern in detail. Figure 10 is the decomposed images of the front and rear of the dense flow at the period 1, 2 and 3. The horizontal axis is the time and the vertical axis is the wavelet levels. The color bar is the same as that in Fig.8. At $64\Delta t$ in Fig.10 (A), indicating the front of the dense flow, values in high level of the levels 6 and 7 are high; however, values in high levels of the levels 3, 4 and 5 are nearly zero. It means high time frequency particles compose the front of the dense flow. Moreover, the particle spatial distribution is located at the upper part of the stationary layer in the high frequency. Precisely, in the level 6, the high value is located at the upper part (denote C) than that just over the stationary layer (denote D) (Takei,M, et al.,1998). It reveals that the particles composing the plug at the front are discharged toward the front air phase. From $65\Delta t$ to $128\Delta t$ when the main body passes, the low level 3 is dominant. At $132\Delta t$, indicating the rear of the dense flow, high particle density is shown in the levels 4 and 5; however, the particle density is low in the levels 5 and 6. As the time goes to $148\Delta t$, the high density is shown in level 6 and 7; however, the particle density is low in the level 5. Moreover, at $156\Delta t$, the high density is shown in only level 7, and then, the high density is disappeared at $157\Delta t$. With regard to the spatial distribution, at $132\Delta t$, a high-density part is located at the top in the level 5; then, the high-density part moves to the middle in the level 6 at $148\Delta t$; and then, the high-density part moves to the bottom in the level

7 at 156Δ*t*. Namely, as the time passes, the dominant level moves from the level 5 to the level 7, and the dominant spatial parts move from the top to the bottom. This tendency is also shown in the period 2 in Fig.10(B) and the period 3 in Fig. 10(C). In detail, at 192Δ*t* at the period 2, the level 6 and the level 7 are high; however, at the rear of the dense flow, the dominant level moves from the level 5 to the level 7; moreover, it moves from the top to the bottom. From the abovementioned discussion, the model of the dense flow is shown in Figure 11. The front of the dense flow is steep, whose part passes through the cross section at high time-period indicating the level 6 and 7. On the other hand, the rear is gently slope, indicating gradually change from the level 4 to the level 7.

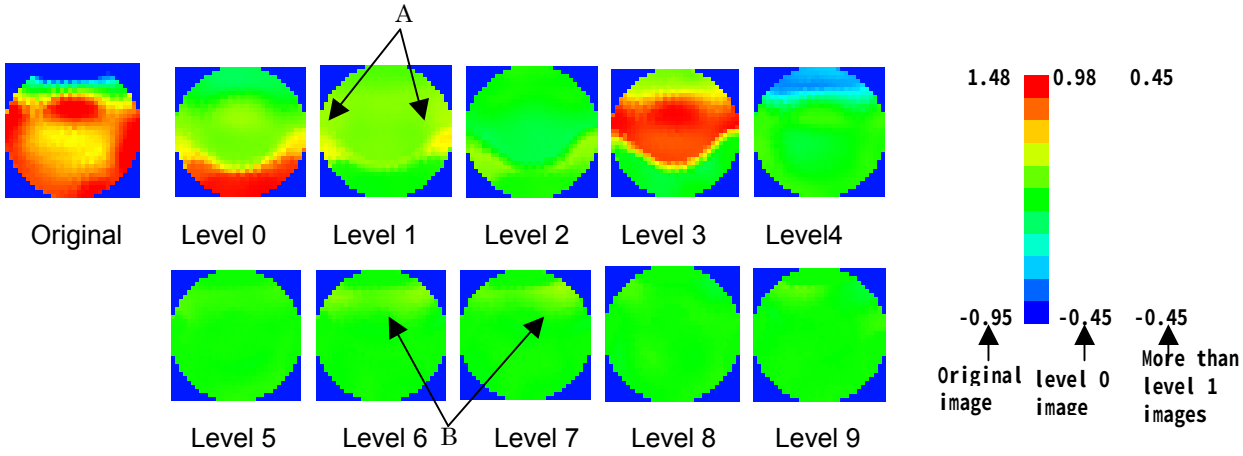

Fig.8 Original image and the decomposed images at 100Δ*t*

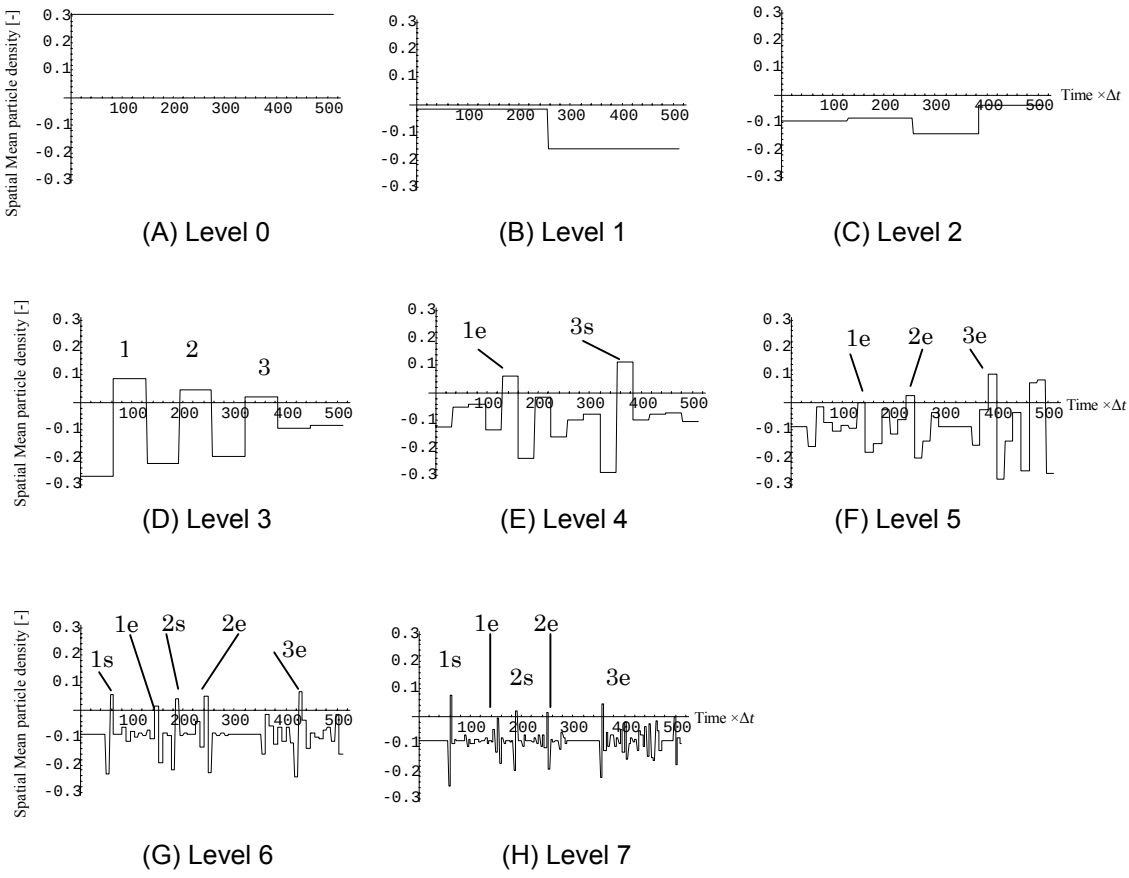

Fig.9 Spatial mean value of decomposed image

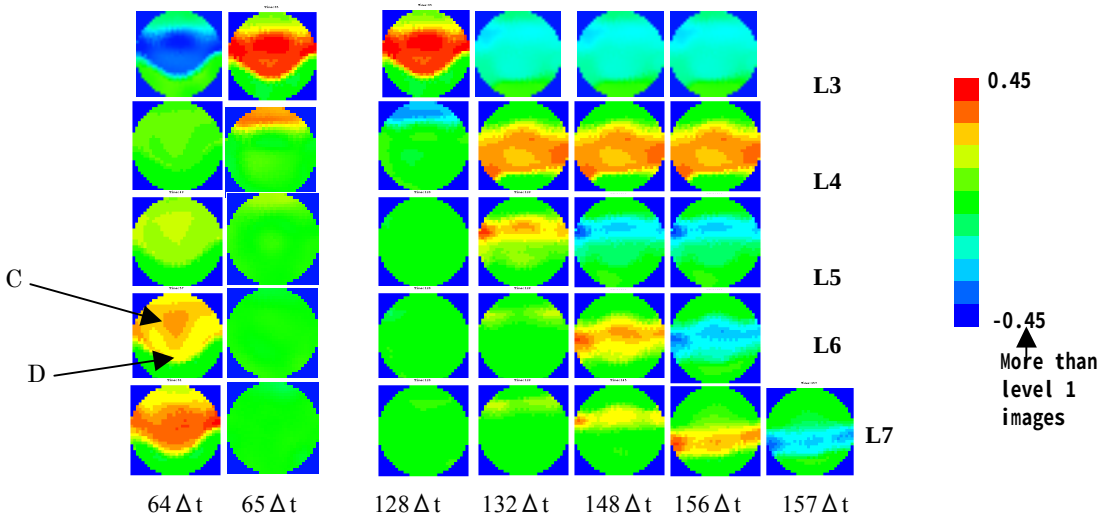

(A) Period 1 time 64-160Δt

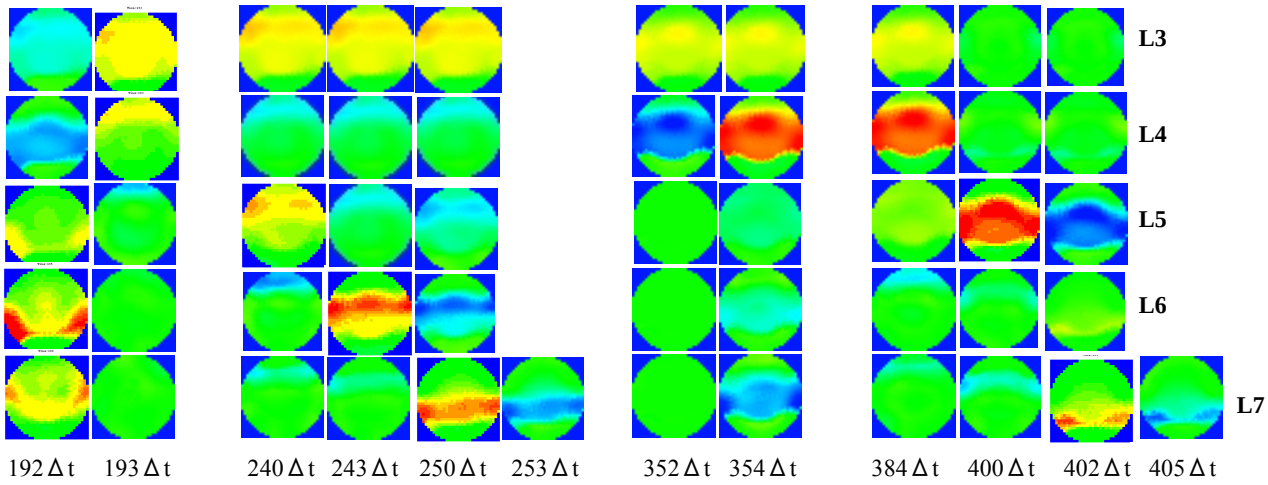

(B) Period 2 time 192-249Δt (C) Period 3 time 352-402Δt

Fig. 10 Front and rear of dense flow

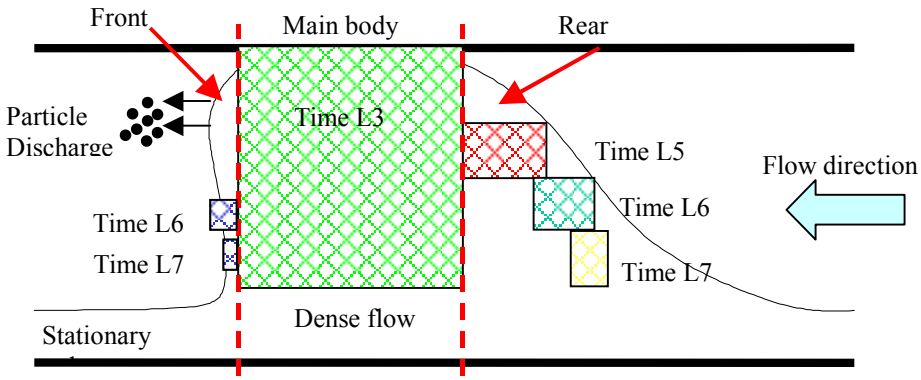

Fig. 11 Model of dense flow

6. Conclusion

The dominant time levels of a dense flow on a pipeline cross section was performed using capacitance-computed tomography and three-dimensional wavelets transform to analyze the particle density of the dense flow at a bend upstream. The following findings were obtained.

(1) The formation of the particle density at the front of a dense flow composes the levels 6 and 7, which indicates the high time frequency level. The high density of the particle spatial distribution is located at the upper part than that just over the stationary layer. It reveals that the particles composing the plug at the front are steep and are discharged toward the front air phase.

(2) The particle density at the rear of the dense flow moves from the level 5 to the level 7; moreover, the dominant spatial part moves from the top to the bottom as the time passes. It indicates the dense flow formation, whose rear is gently slope.

The authors wish to thank Dr. Tomasz Dyakowski of UMIST and Mr. Malcolm Byars of PTL in UK for useful advice.

References

Dyakowski,T., Luke,S.P., Ostrowski,K.L. and Williams,R.A. (1999) On-Line Monitoring of Dense Phase Flow Using Real Time Dielectric Imaging, *Powder technol*, 104, pp.287-295.

Huang,S.M., Plaskowski,A.B., Xie,C.G., and Beck,M.S. (1989) Tomographic Imaging of Two-Component Flow Using Capacitance Sensors, *J.Phys, E: Sci, Intrrum*, 22, pp.173-177

Klinzing G.E, (2001) Dense Phase (plug) Conveying –Observations and Projections--, *Handbook of Conveying and Handling of Particulate Solids*, Edited by A.Levy, and H.Kalman, Elsevier Science B.V., pp329-341

Li,H., Takei, M., Ochi, M., Saito, Y. and Horii, K. (1999) Application of Two-dimensional Orthogonal Wavelets to Multiresolution Image Analysis of a Turbulent Jet, *Transactions of the Japan Society for Aeronautical and Space Sciences*, Vol.42, No.137, pp.120-127.

Takei,M, Ochi,M. et al. (1998) Movement of Particles Composing Plug at Front End, *Transactions of the Japan Society of Mechanical Engineers*, Vol64, No.628, pp.86-92